Journal of Sound and Vibration (2002) **257**(1), 157–175
doi:10.1006/jsvi.5036, available online at http://www.idealibrary.com on IDEAL®

CONTROL DESIGN OF ACTIVE VIBRATION ISOLATION USING μ-SYNTHESIS

M. R. Bai and W. Liu

Department of Mechanical Engineering, National Chiao-Tung University, 1001 *Ta-Hsueh Road, Hsin-Chu* 30050, *Taiwan, People's Republic of China. E-mail*: *msbai@cc.nctu.edu.tw*

(*Received* 19 *July* 2001, *and in final form* 3 *January* 2002)

Numerical and experimental investigations on active vibration isolation system are presented in this paper. Two configurations are implemented for a statically balanced three-mount system. To reduce the influence of payload dynamics and coupling among the control actuators, intermediate masses are added to the system. Linear quadratic Gaussian control and μ-synthesis are employed in the controller synthesis. The controllers are implemented on the platform of a floating-point digital signal processor. The results obtained from simulations and experiments indicated that the optimal controllers achieved the desired performance under the constraint of robust stability.

1. INTRODUCTION

Vibration isolation system is often required in protecting high-tech equipment such as those used in semiconductor manufacturing industry, where high precision of machining is crucial. Use of passive isolators has been the common practice to isolate vibration from the floor in that passive systems are easy to design and install. However, in the conventional passive design, a trade-off exists between the isolation performance in the low- and high-frequency regions. To reduce the response at resonance, damping treatment is often applied at the expense of degradation of isolation at high frequencies [1]. Alternatively, isolation of vibration can be achieved by active means by introducing secondary vibration sources to the original system. This approach has been found to be more effective, particularly in low frequencies, than the passive control [1].

There have been many studies devoted to the subject of active isolation system. Karnopp *et al.* proposed an inertial or "skyhook" damping idea to bypass the aforementioned trade-off in relative velocity damping [1]. Beard *et al.* presented an active hard-mount strategy to achieve desired performance and stability robustness [2]. Sievers and von Flotow developed two methods based on linear quadratic Gaussian (LQG) control: disturbance rejection via disturbance modelling and LQG control with frequency-shaped cost function [3]. Watanabe *et al.* developed a levitated vibration isolation system using H_∞ synthesis and PI control with relative displacement feedback [4]. Kim *et al.* developed a decentralized control scheme using the positive real property of the system for active vibration isolation [5].

This paper investigates two configurations and two algorithms in the context of active vibration isolation control. The major difference between two configurations is whether or not intermediate masses are introduced. As shall be seen later, intermediate masses are useful in decoupling the influence due to payload dynamics and interactions among active

0022-460X/02/$35.00

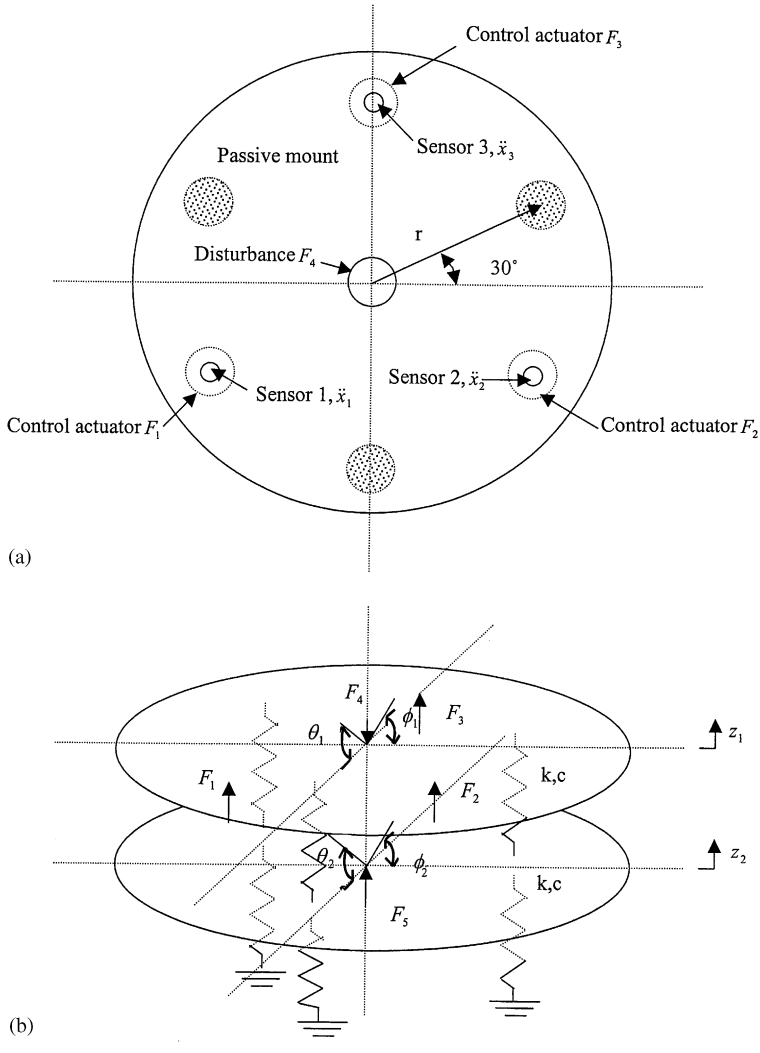

Figure 1. The model of the vibration isolation system: (a) top view; (b) side view.

mounts, which could destabilize the system. Two control algorithms, the LQG control and the μ synthesis, are employed in the controller design. The controllers are implemented on the plateform of a floating-point digital signal processor (DSP). The results obtained from numerical simulations and experimental verifications are also discussed.

2. SYSTEM MODELLING

The model of the vibration isolation system shown in Figure 1 consists of two circular platforms, six passive mounts, and three sets of collocated accelerometers and electromagnetic actuators. The upper platform serves as the isolation table, while the lower platform serves as the vibrating floor. There are two sources of disturbance acting on the system. One for modelling the disturbance from the payload is located at the center of the upper platform, and the other for modelling the disturbance from the floor is located at the center of the lower platform.

For the system depicted in Figure 1, variational principles are employed in deriving the equations of motion [6]. The symbols used in the derivation are summarized as follows: T, V the kinetic energy and potential energy of the system, m_1, m_2 the masses of the upper and lower platforms, respectively, I_1, I_2 the moment of inertias of the upper and lower platforms, respectively, k, c the spring and damping coefficients of the passive mounts, z_1, z_2 the displacements of the isolation table and floor, θ_1, ϕ_1, θ_2, ϕ_2 the angular displacements of the isolation table and floor, r the radius of platform, F_1, F_2, F_3 the control forces of actuators, F_4, F_5 the payload disturbance and floor disturbance, and q_j, Q_j: generalized co-ordinate and generalized force.

Define the generalized co-ordinates z_1, z_2, θ_1, θ_2, ϕ_1 and ϕ_2. Assume that the amplitude of vibration is small such that the non-linear terms are negligible. The Lagrange equation

$$\frac{\mathrm{d}}{\mathrm{d}t}\left(\frac{\partial L}{\partial \dot{q}_j}\right) - \frac{\partial L}{\partial q_j} = Q_j, \quad j = 1, 2, \ldots, 6 \tag{1}$$

where the Lagrangian $L = T - V$, is used for obtaining the following equations of motion:

$$\begin{aligned}
m_1\ddot{z}_1 &= -3k(z_1 - z_2) + F_1 + F_2 + F_3 - F_4 - 3c\dot{z}_1\\
I_1\ddot{\phi}_1 &= -\frac{3}{2}kr^2(\phi_1 - \phi_2) + \frac{\sqrt{3}}{2}r(-F_1 + F_2) - \sqrt{3}rc\dot{\phi}_1\\
I_1\ddot{\theta}_1 &= -\frac{3}{2}kr^2(\theta_1 - \vartheta_2) + \frac{r}{2}(F_1 + F_2) - rF_3 - 2rc\dot{\theta}_1\\
m_2\ddot{z}_2 &= 3k(z_1 - 2z_2) + F_5 - 6c\dot{z}_2\\
I_2\ddot{\phi}_2 &= \tfrac{3}{2}kr^2(\phi_1 - 2\phi_2) - 2\sqrt{3}rc\dot{\phi}_2\\
I_2\ddot{\theta}_2 &= \tfrac{1}{2}kr^2(\theta_1 - 2\theta_2) - 4rc\dot{\theta}_2.
\end{aligned} \tag{2}$$

In order for the subsequent use of active control design, the equations of motion are converted into the state-space form

$$\dot{\mathbf{x}} = \mathbf{A}\mathbf{x} + \mathbf{B}\mathbf{u}, \qquad \mathbf{y} = \mathbf{C}\mathbf{x} + \mathbf{D}\mathbf{u} \tag{3}$$

where state variables $\mathbf{x} = [z_1, \dot{z}_1, z_2, \dot{z}_2, \theta_1, \dot{\theta}_1, \theta_2, \dot{\theta}_2, \phi_1, \dot{\phi}_1, \phi_2, \dot{\phi}_2]^{\mathrm{T}}$, control force $\mathbf{u} = [F_1 \ F_2 \ F_3 \ F_4 \ F_5]^{\mathrm{T}}$, $\mathbf{y}$ is a column vector consisting of the accelerations measured by the sensors, the system matrices

$$\mathrm{A} = \begin{bmatrix}
0 & 1 & 0 & 0 & 0 & 0 & 0 & 0 & 0 & 0 & 0 & 0\\
-\frac{3k}{m_1} & -\frac{3c}{m_1} & 0 & 0 & 0 & 0 & \frac{3k}{m_1} & 0 & 0 & 0 & 0 & 0\\
0 & 0 & 0 & 1 & 0 & 0 & 0 & 0 & 0 & 0 & 0 & 0\\
0 & 0 & -\frac{3kr^2}{2I_1} & -\frac{\sqrt{3}rc}{I_1} & 0 & 0 & 0 & 0 & \frac{3kr^2}{2I_1} & 0 & 0 & 0\\
0 & 0 & 0 & 0 & 0 & 1 & 0 & 0 & 0 & 0 & 0 & 0\\
0 & 0 & 0 & 0 & -\frac{3kr^2}{2I_1} & -\frac{2rc}{I_1} & 0 & 0 & 0 & 0 & \frac{3kr^2}{2I_1} & 0\\
0 & 0 & 0 & 0 & 0 & 0 & 0 & 1 & 0 & 0 & 0 & 0\\
3\frac{k}{m_2} & 0 & 0 & 0 & 0 & 0 & -\frac{6k}{m_2} & -\frac{6c}{m_2} & 0 & 0 & 0 & 0\\
0 & 0 & 0 & 0 & 0 & 0 & 0 & 0 & 0 & 1 & 0 & 0\\
0 & 0 & \frac{3kr^2}{2I_2} & 0 & 0 & 0 & 0 & 0 & -\frac{3kr^2}{I_2} & -\frac{2\sqrt{3}kr^2}{I_2} & 0 & 0\\
0 & 0 & 0 & 0 & 0 & 0 & 0 & 0 & 0 & 0 & 0 & 1\\
0 & 0 & 0 & 0 & \frac{3kr^2}{2I_2} & 0 & 0 & 0 & 0 & 0 & -\frac{3kr^2}{I_2} & -4\frac{rc}{I_2}
\end{bmatrix},$$

$$\mathbf{B} = \begin{bmatrix} 0 & 0 & 0 & 0 & 0 \\ \frac{1}{m_1} & \frac{1}{m_1} & \frac{1}{m_1} & -\frac{1}{m_1} & 0 \\ 0 & 0 & 0 & 0 & 0 \\ -\frac{\sqrt{3}r}{2I_1} & \frac{\sqrt{3}r}{2I_1} & 0 & 0 & 0 \\ 0 & 0 & 0 & 0 & 0 \\ \frac{r}{2I_1} & \frac{r}{2I_1} & -\frac{r}{I_1} & 0 & 0 \\ 0 & 0 & 0 & 0 & 0 \\ 0 & 0 & 0 & 0 & \frac{1}{m_2} \\ 0 & 0 & 0 & 0 & 0 \\ 0 & 0 & 0 & 0 & 0 \\ 0 & 0 & 0 & 0 & 0 \end{bmatrix},$$

$$\mathbf{C} = \begin{bmatrix} -\frac{3k}{m_1} & -\frac{3c}{m_1} & \frac{3\sqrt{3}kr^3}{4I_1} & \frac{3cr^2}{2I_1} & -\frac{3kr^3}{4I_1} & -\frac{cr^2}{I_1} & \frac{3k}{m_1} & 0 & -\frac{3\sqrt{3}kr^3}{4I_1} & 0 & \frac{3kr^3}{4I_1} & 0 \\ -\frac{3k}{m_1} & -\frac{3c}{m_1} & \frac{3\sqrt{3}kr^3}{4I_1} & \frac{3cr^2}{2I_1} & \frac{3kr^3}{4I_1} & -\frac{cr^2}{I_1} & \frac{3k}{m_1} & 0 & -\frac{3\sqrt{3}kr^3}{4I_1} & 0 & \frac{3kr^3}{4I_1} & 0 \\ -\frac{3k}{m_1} & -\frac{3c}{m_1} & 0 & 0 & \frac{3kr^3}{2I_1} & \frac{2cr^2}{I_1} & \frac{3k}{m_1} & 0 & 0 & 0 & \frac{3kr^3}{2I_1} & 0 \end{bmatrix},$$

$$\mathbf{D} = \begin{bmatrix} \frac{1}{m_1} + \frac{r^2}{I_1} & \frac{1}{m_1} - \frac{r^2}{2I_1} & \frac{1}{m_1} - \frac{r^2}{2I_1} & -\frac{1}{m_1} & 0 \\ \frac{1}{m_1} - \frac{r^2}{2I_1} & \frac{1}{m_1} + \frac{r^2}{I_1} & \frac{1}{m_1} - \frac{r^2}{2I_1} & -\frac{1}{m_1} & 0 \\ \frac{1}{m_1} - \frac{r^2}{2I_1} & \frac{1}{m_1} - \frac{r^2}{2I_1} & \frac{1}{m_1} + \frac{r^2}{I_1} & -\frac{1}{m_1} & 0 \end{bmatrix}.$$

3. CONTROLLER SYNTHESIS

The methods for controller synthesis employed in this paper are LQG control and μ-synthesis in state-space control theory. The need for the seemingly complicated control strategies is motivated by the fact that large number of modes including structural modes are present in the dynamics and strong coupling exists between each sensor–actuator pair. Although the system is symmetric and driven in the center, the controller is still based on a multiple-input–multiple-output (MIMO) design. This general configuration is at first glance an overkill, but is necessary for experimental verification of the active-control system, where rocking is inevitable due to some practical reasons, e.g., imperfect symmetry. In reality, the "collocated" three pairs of frequency response functions would never be identical. We need an automatic means to design the controller because of large number of modes; we also need a controller within a MIMO framework because of the strong coupling. LQG control and μ-synthesis are two such methods well suited for these purposes.

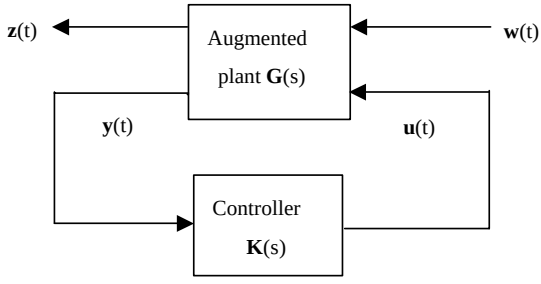

Figure 2. Generalized feedback control structure.

Because LQG control is a well-known control method, its review is omitted here. For details, one may consult Reference [7]. As compared to the LQG method, μ-synthesis provides a more robust and comprehensive design that achieves the performance and the stability bounds as well, by choosing appropriate frequency weighting on system perturbations and uncertainties. In this section, the general ideas of μ-synthesis will be given, alongside a brief review of H_∞ control theory for it is the basis of the former theory.

3.1. H_∞ ROBUST CONTROL

The H_∞ theories can be found in much control literature and we present only the key ones needed in the analysis of our problem. The rest are mentioned without proof.

In modern control theory, all control structures can be cast into a generalized control framework, as depicted in Figure 2. The framework contains a controller $\mathbf{K}(s)$ and an augmented plant $\mathbf{P}(s)$ in which $\mathbf{z}(t)$ is a vector signal including all controlled signals and tracking errors, $\mathbf{w}(t)$ is a vector signal including noise, disturbances, and reference signal, $\mathbf{u}(t)$ is the control signal, and $\mathbf{y}(t)$ is the measurement output.

$$\begin{bmatrix}\mathbf{Z}(s)\\ \mathbf{Y}(s)\end{bmatrix} = \mathbf{P}(s)\begin{bmatrix}\mathbf{W}(s)\\ \mathbf{U}(s)\end{bmatrix} = \begin{bmatrix}\mathbf{P}_{11}(s) & \mathbf{P}_{12}(s)\\ \mathbf{P}_{21}(s) & \mathbf{P}_{22}(s)\end{bmatrix}\begin{bmatrix}\mathbf{W}(s)\\ \mathbf{U}(s)\end{bmatrix}$$

$$\mathbf{U}(s) = \mathbf{K}(s)\mathbf{Y}(s) \tag{4}$$

where the submatrices $\mathbf{P}_{ij}(s)$ are compatible partition of the augmented plant $\mathbf{P}(s)$. Let the transfer function matrix from $\mathbf{W}(s)$ to $\mathbf{Z}(s)$ be denoted by $\mathbf{T}_{zw}(s)$ that can be expressed by linear fraction transformation (LFT)

$$\mathbf{T}_{zw}(s) = F_l(\mathbf{P}, \mathbf{K}) = \mathbf{P}_{11}(s) + \mathbf{P}_{12}(s)\mathbf{K}(s)[\mathbf{I} - \mathbf{P}_{22}(s)\mathbf{K}(s)]^{-1}\mathbf{P}_{21}(s). \tag{5}$$

The H_∞ control problem amounts to finding a stabilizing controller $\mathbf{K}$ that minimizes

$$\|\mathbf{T}_{zw}(s)\|_\infty = \sup_{-\infty \leqslant \omega \leqslant \infty} \bar{\sigma}\ [\mathbf{T}_{zw}(\mathrm{j}\omega)]. \tag{6}$$

Finding an optimal H_∞ controller, however, is generally very difficult. In practice, it is usually easier to obtain a "suboptimal" controller. That is, for a given $\gamma > 0$, we seek to find a stabilizing controller such that

$$\|\mathbf{T}_{zw}(s)\|_\infty < \gamma. \tag{7}$$

The details of the synthesis procedure of the H_∞ controllers can be found in references [8, 9] and are omitted here for simplicity.

3.2. μ-SYNTHESIS

The aforementioned H_∞ tends to be conservative since it does not take into account the structure of uncertainties. A less conservative design would be to use μ-synthesis. The μ-analysis problem involves determining whether a control system remains within the stability and performance bounds and the controlled signals remain small, in the presence of exogenous inputs and norm-bounded perturbations and uncertainties [10]. Assume that the uncertainty model Δ belongs to the set

$$\Delta = \text{diag}(\delta_1 \mathbf{I}_{k_1}, \ldots, \delta_r \mathbf{I}_{k_r}, \Delta_1, \Delta_2, \ldots, \Delta_s)\colon \delta_i \in \mathbf{C}, \quad \Delta_j \in \mathbf{C}^{m_j \times m_i}, \tag{8}$$

$$B\Delta = \Delta \in \Delta | \bar{\sigma}(\Delta) \leqslant 1. \tag{9}$$

There are two types of uncertainty model Δ: blocks-repeated scalar and full blocks. Two non-negative integers, r and s, represent the number of repeated scalar blocks and the number of full blocks respectively. The dimension of the ith repeated scalar blocks is $k_r \times k_r$, hile the jth full block is $m_j \times m_i$. In equation (9), $\bar{\sigma}$ denotes the maximum singular value. For a system $\mathbf{M}$, the structured singular value μ is defined as

$$\mu_\Delta(\mathbf{M}) = \left(\min_{\Delta \in \Delta} \{ \bar{\sigma}(\Delta)\colon det(\mathbf{I} - \Delta\mathbf{M}) = 0 \} \right)^{-1} \tag{10}$$

which is essentially a measure of the smallest uncertainty Δ that may destabilize the closed-loop system. The ultimate goal of the μ-synthesis lies in finding a controller to achieve the so-called robust performance, which implies that the performance specifications of the closed-loop system are met for all uncertainty models. The condition of robust performance is the linear fractional transformation $F_u(\mathbf{G}, \Delta)$ is stable for all $\Delta \in B\Delta$ and its infinity norm is less than 1 $\| F_u(\mathbf{G}, \Delta) \|_\infty < 1$.

Figure 3(a) illustrates the block diagram of the system which can be rearranged into the μ-synthesis framework in Figure 3(b). In the figure, $\mathbf{G}$ is the augmented plant described by the input–output relation

$$\begin{bmatrix} \boldsymbol{\Delta}_{in} \\ \mathbf{z}_1 \\ \mathbf{z}_2 \\ \mathbf{y} \end{bmatrix} = \mathbf{G} \begin{bmatrix} \boldsymbol{\Delta}_{out} \\ \mathbf{d} \\ \mathbf{u} \end{bmatrix} = \begin{bmatrix} 0 & 0 & \mathbf{W}_{mult} \\ \mathbf{W}_{per} & \mathbf{W}_{per} & \mathbf{W}_{per}\mathbf{P} \\ 0 & 0 & \mathbf{W}_c \\ \mathbf{I} & \mathbf{I} & \mathbf{P} \end{bmatrix} \begin{bmatrix} \boldsymbol{\Delta}_{out} \\ \mathbf{d} \\ \mathbf{u} \end{bmatrix}. \tag{11}$$

The term $\mathbf{W}_{per}$ is a performance weight for disturbance rejection in the desired frequency band. In our case, $\mathbf{W}_{per}$ is chosen to be a band-pass filter. The nominal plant $\mathbf{P}$ together with uncertainty models $\boldsymbol{\Delta}$ defines a set of plants $\tilde{\mathbf{P}}$ within which the real physical system is assumed to lie. In our case, the frequency response measured by the signal analyzer represents the perturbed plant $\tilde{\mathbf{P}}$ and the identified model represents the nominal plant $\mathbf{P}$. A frequency-domain multiplicative type of uncertainty is used. The relation between the perturbed model set $\tilde{\mathbf{P}}$ and the nominal plant $\mathbf{P}$ is

$$\tilde{\mathbf{P}} = (\mathbf{I} + \Delta)\mathbf{P} \tag{12}$$

or

$$\Delta = \mathbf{P}^{-1}\tilde{\mathbf{P}} - \mathbf{I}. \tag{13}$$

The uncertainty weight satisfies

$$\bar{\sigma}\{ \Delta(\mathrm{j}\omega) \} < |\mathbf{W}_{mult}(\mathrm{j}\omega)| \quad \forall \omega. \tag{14}$$

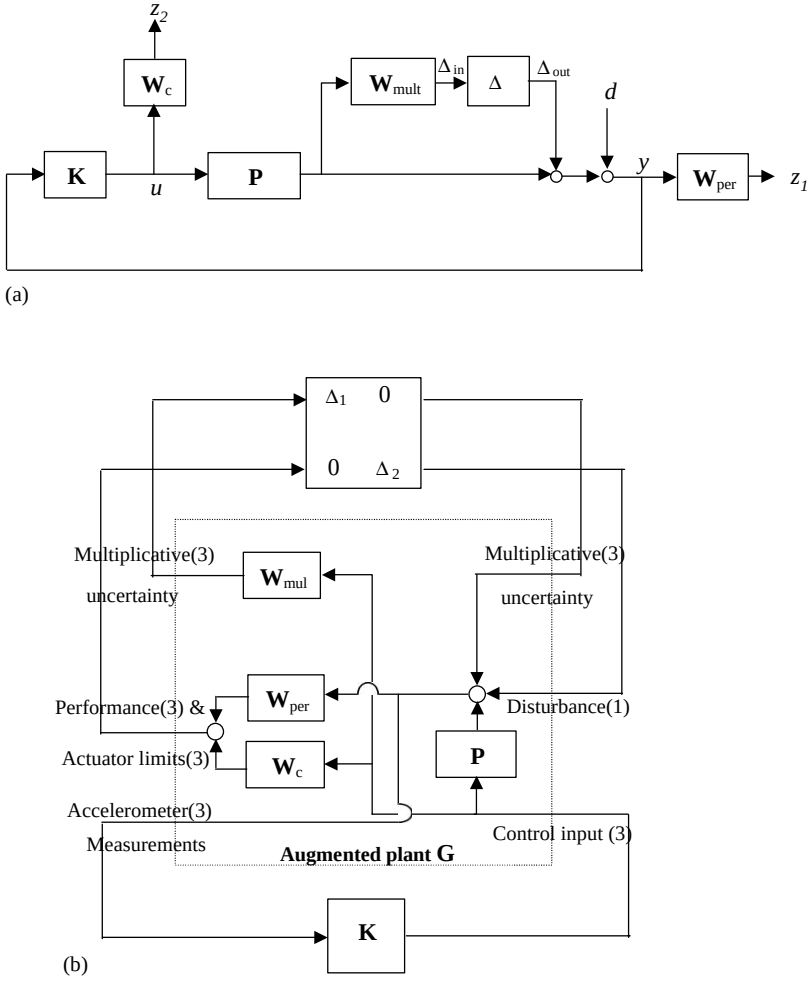

Figure 3. Block diagram of the closed-loop system: (a) original block diagram; (b) generalized feedback control structure for μ-synthesis.

To prevent the system from instability, the controller gain should be restricted at high frequencies. In this work, we use a high-pass filter as the controller weight $\mathbf{W}_c$.

The objective of μ-synthesis is to find a stabilizing controller such that the closed-loop system achieves robust performance, i.e.,

$$\sup_{\omega \in R} \mu_{\Delta_F}[\mathbf{G}(jw)] < 1, \tag{15}$$

where $\Delta_F = \text{diag}(\mathbf{\Delta}_1, \mathbf{\Delta}_2)$, $\mathbf{\Delta} \in B\mathbf{\Delta}$. Like H_∞ control, it is very difficult to find an optimal solution satisfying the criterion in equation (15). A practical remedy to this problem is the so-called *D-K iteration* technique. This method uses H_∞ controller and weighting matrices as the starting point of the iteration procedure. In general, it takes only a few iterations to reach a suboptimal solution. The details of μ analysis and synthesis can be found in reference [10].

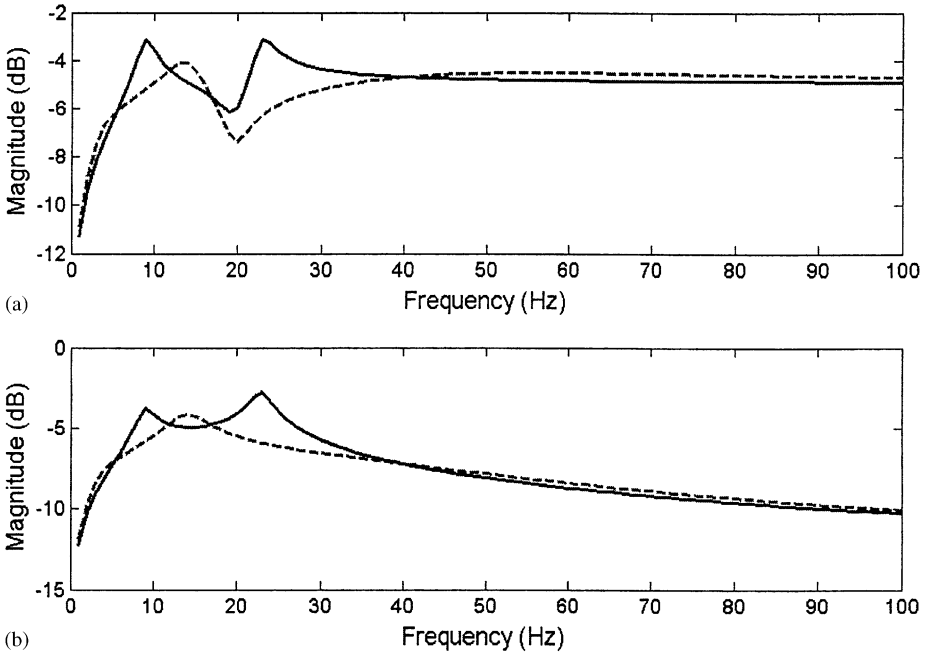

Figure 4. The simulation results of frequency responses (m/N s^2) from disturnances to acclerometer 1 obtained usin LQG control: (a) payload disturbance; (b) floor disturbance (——, control off; – – – –, control on).

4. NUMERICAL AND EXPERIMENTAL INVESTIGATIONS

Numerical simulations and experimental investigations were carried out to verify the aforementioned control methods applied to the vibration isolation problem. First, a numerical simulation is conducted. In the simulation, the isolation table is assumed to be a circular plate with a diameter 1 m, thickness 15 mm, and mass 5 kg. The passive mounts has stiffness $k = 4550$ N/m and damping $c = 147$ Ns/m. LQG controllers are designed on the basis of the state-space model derived in section 2. The frequency responses (m/N s^2) from disturnances to acclerometer 1 are shown in Figure 4. Attenuation can be observed in two separate bands, 7–12 and 18–40 Hz. The maximum attenuation is found to be 3·5 dB for the floor disturbance. Some amplification can also be seen in the band 12–18 Hz.To improve the performance, a second order *internal model* is introduced in the control loop [11]

$$M(s) = \frac{100s}{s^2 + 23{\cdot}88s + 14250}, \tag{16}$$

where the resonant frequency is set to be 19 Hz and the damping ratio is set to be 10%. The parameters of the LQG controller are $\mathbf{Q}_c = 1000\mathbf{I}_{17\times17}$, $\mathbf{R}_c = \mathbf{I}_{17\times17}$, $\mathbf{Q}_f = 600\mathbf{I}_{3\times3}$, and $\mathbf{R}_f = \mathbf{I}_{3\times3}$. Figure 5 shows the block diagram of the total system. The frequency responses (m/N s^2) from disturnances to acclerometer 1 are shown in Figure 6. Attenuation can be observed in a more concentrated band, 11–36 Hz. Furthermore, no adverse amplification is observed in this case. Thus, with the use of the internal model, the control bandwidth tends to be more concentrated without adverse amplification of disturbances.

In addition to the numerical simulations, experiments are carried out to investigate the proposed active vibration isolation system. Two configurations of the isolation system are

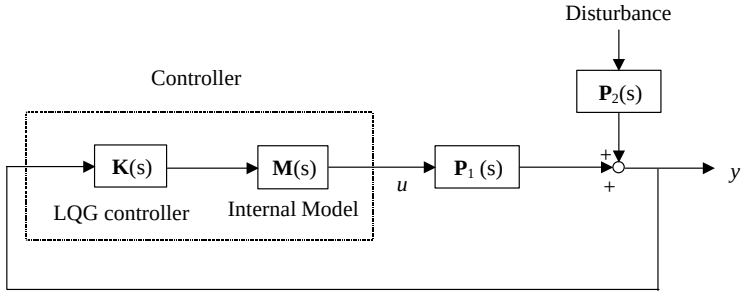

Figure 5. The block diagram of the LQG control with internal model.

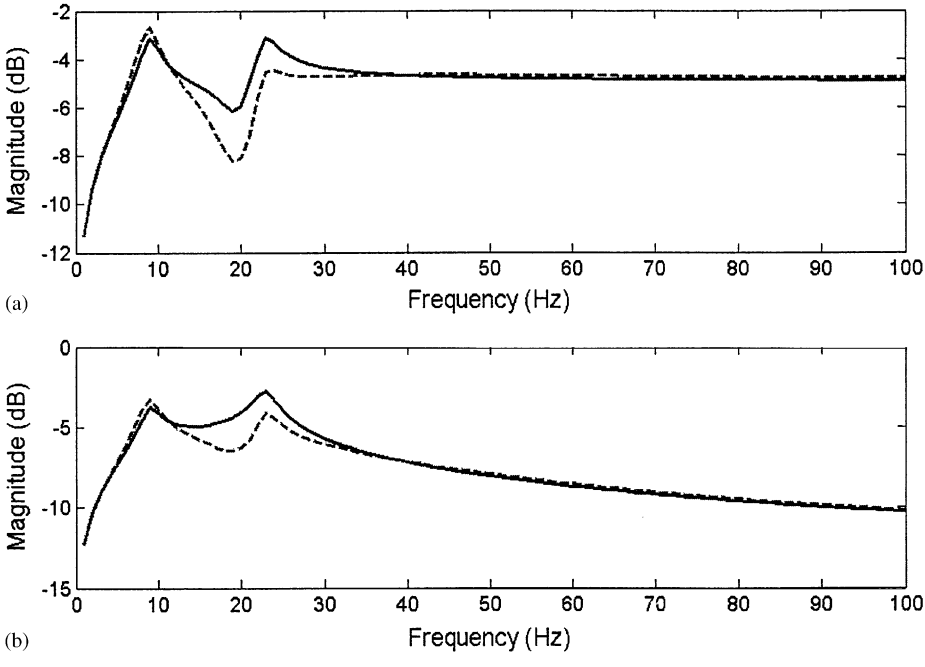

Figure 6. The simulation results of frequency responses ($m/N\,s^2$) from disturnances to acclerometer 1 obtained using LQG with internal model: (a) payload disturbance; (b) floor disturbance (——, control off: – – – –, control on).

implemented in the experiments. Configuration 1 is shown in Figure 7, where the isolation table is supported by three passive mounts and three electromagnetic actuators. The isolation table is a circular plate with a diameter 1 m, thickness 15 mm, and mass 5 kg. Three sets of collocated seismic accelerometers (PCB 393A03) and electromagnetic actuators are used in the system. Similar to the principles of loudspeakers and vibration shakers, the actuator operates primarily by means of electromagnetic interactions between a voice coil and a permanent magnet. A Nd–Fe–B cylindrical magnet is used to generate high-flux-density magnetic field. Each actuator has equivalent stiffness $k_a = 4550\,N/m$ and damping ca $= 147\,Ns/m$. In addition, two electromagnetic actuators located at the center of the plates serve as the disturbance sources acting on the paylaod and the floor respectively.

Configuration 2 is shown in Figure 8(a). The experimental set-up is shown in Figure 8(b). In the configuration, the intermediate masses are square boards of dimensions

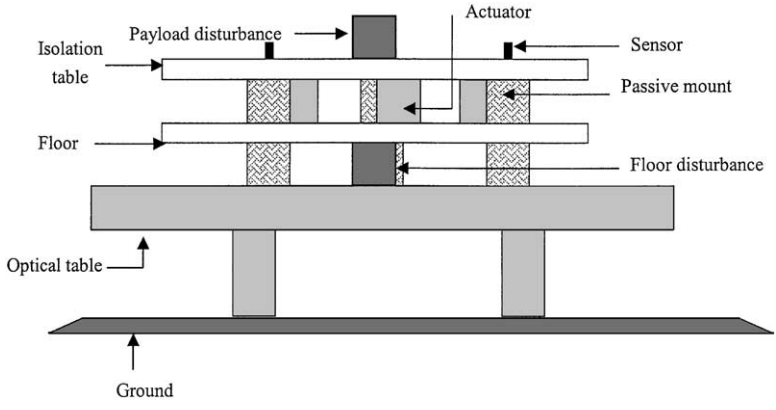

Figure 7. The experimental rig of configuration 1.

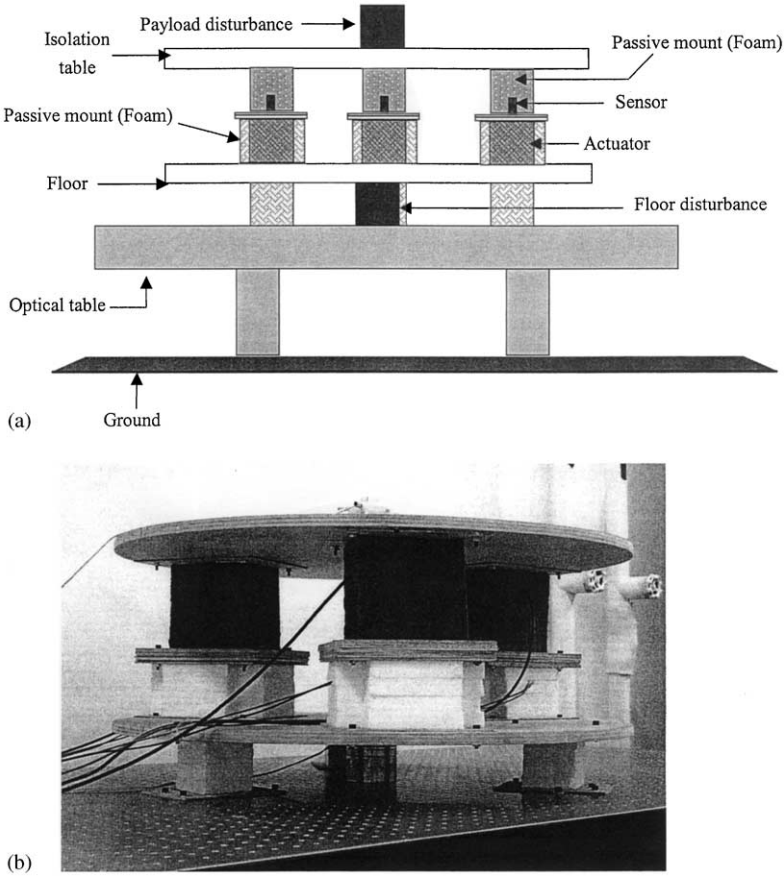

Figure 8. The experimental rig of configuration 2: (a) schematic diagram; (b) photo.

$220 \times 200 \times 20\,\text{mm}^3$. The passive mount above the intermediate mass is a square PU-foam block softer than the passive mount below the intermediate mass. The system dynamics of entire experimental arrangement is apparently more complex than the discrete rigid-body

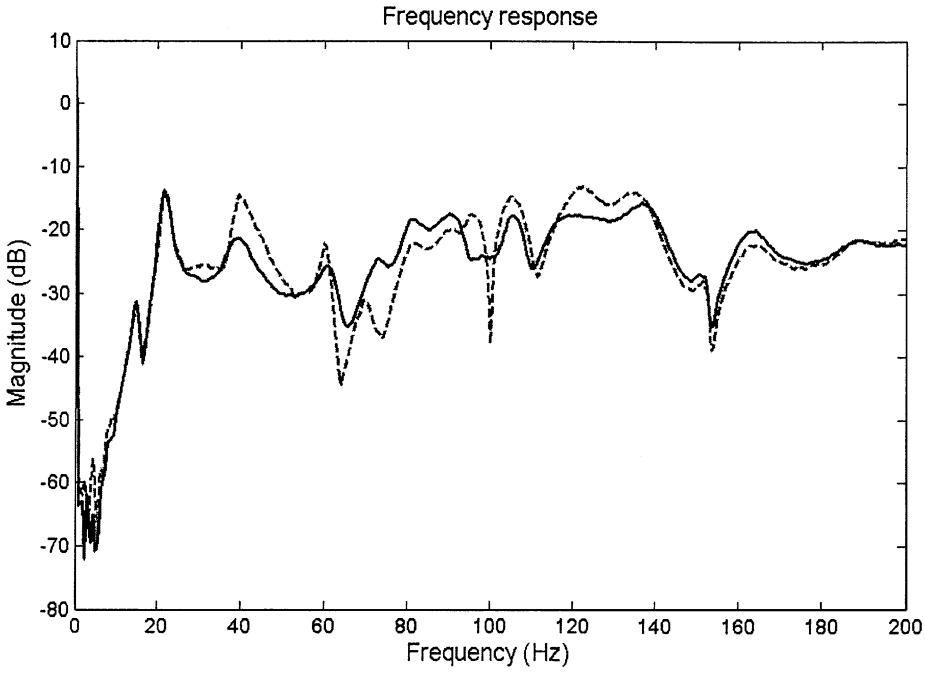

Figure 9. The experimental result of configuration 1 obtained using LQG control with internal model (——, control off, – – – –, control on).

model used in the numerical simulation. Unmodelled dynamics, mostly structural dynamics, of the platforms and the passive mounts have pronounced effects on the physical system. Apart from the complexity of structural modes, it is very difficult if not impossible to identify within acceptable accuracy the meterial properties and transducer dynamics such that the overall system dynamics can be fully accounted for. Instead of structrual dynamic view point, this paper regress to adopt a more control system-oriented approach, eigensystem realization algorithm (ERA). ERA is able to extract the modal parameters, based on the minimum realization of the MIMO sysetm in question [12]. The method *per se* is an experimental system identification approach that may provide little physical insight, yet a practical and effective method for capturing the overall dynamics of a realistic system, including the physical system (platforms and passive mounts), sensors (accelerometers), actuators (voice-coil excitors), etc.

4.1. EXPERIMENTAL RESULTS OF CONFIGURATION 1

A LQG controller with internal model is designed and implemented by using a DSP. The parameters of LQG controller are $\mathbf{Q}_c = 200 \times \mathbf{I}_{26\times 26}$, $\mathbf{R}_c = \mathbf{I}_{3\times 3}$, $\mathbf{Q}_f = 150 \times \mathbf{I}_{3\times 3}$, and $\mathbf{R}_f = \mathbf{I}_{3\times 3}$. The discrete-time transfer function of the internal model is

$$H(z) = \frac{0{\cdot}1556z^2 - 0{\cdot}1556}{z^2 - 1{\cdot}187z + 0{\cdot}8137} \tag{17}$$

which corresponds to the resonanance frequency 70 Hz and damping ratio 12%. The experimental result is shown in Figure 9. In our control problem, it is in the same way to deal with the disturbance from payload and floor. Hereafter, we show only the experimental results of rejection of the disturbance from the floor. Attenuation is found in the frequency

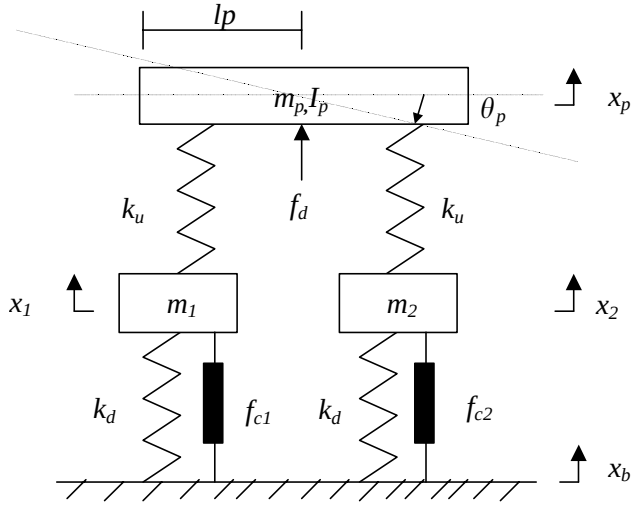

Figure 10. The simulation model with intermediate masses.

range 60–92 and 140–185 Hz.The maximum attenuation is 13 dB. However, in frequency range 25–52 and 82–128 Hz, the disturbance is slightly amplified due to the *waterbed effect* [13]. The waterbed effect is essentially a control spill-over as well as a physical constraint imposed by non-minimum phase zeros of a system. For a given system configuration, this constraint is fixed and unavoidable. Nevertheless, one can usually manipulate the type and position of sensors and actuators to alter the zeros of a system, so that the waterbed effect can be alleviated. For example, collocation of sensors and actuators is a common approach for mitigating the waterbed effect.

4.2. EFFECTS OF THE INTERMEDIATE MASSES

A modification is made to the system of configuration 1 by introducing intermediate masses to the mounts. The purpose of this approach is two-fold. First, the influence of payload dynamics can be reduced. Second, the interactions among the actuators can be decoupled. In a multivariable system as in our case, every input controls more than one output and every output is controlled by more than one input. Because of this phenomenon, which is called coupling or interaction, it is in general very difficult to control a mulitivariable system. Therefore, one seeks whenever possible to "decouple" either electronically or mechanically a multivariable system such that every input controls only one output and every output is controlled by only one input. Consequently, a decoupled system can be regarded as consisting of a set of independent single-variable systems and the resulting system transfer function matrix becomes nearly diagonal [11].

Consider a simplified system of Figure 10. The equations of motion are

$$\begin{bmatrix} m_p & 0 & 0 & 0 \\ 0 & I_p & 0 & 0 \\ 0 & 0 & m_1 & 0 \\ 0 & 0 & 0 & m_2 \end{bmatrix} \begin{bmatrix} \ddot{x}_p \\ \ddot{\theta}_p \\ \ddot{x}_1 \\ \ddot{x}_2 \end{bmatrix} + \begin{bmatrix} 2k_u & 0 & -k_u & -k_u \\ 0 & 2k_u l_p^2 & -k_u l_p & k_u l_p \\ -k_u & -k_u l_p & k_u + k_d & 0 \\ -k_u & k_u l_p & 0 & k_u + k_d \end{bmatrix} \begin{bmatrix} x_p \\ \theta_p \\ x_1 \\ x_2 \end{bmatrix} = \begin{bmatrix} 1 & 0 & 0 & 0 \\ 0 & 0 & 0 & 0 \\ 0 & k_d & 1 & 0 \\ 0 & k_d & 0 & 1 \end{bmatrix} \begin{bmatrix} F_p \\ x_b \\ F_{c1} \\ F_{c2} \end{bmatrix}. \tag{18}$$

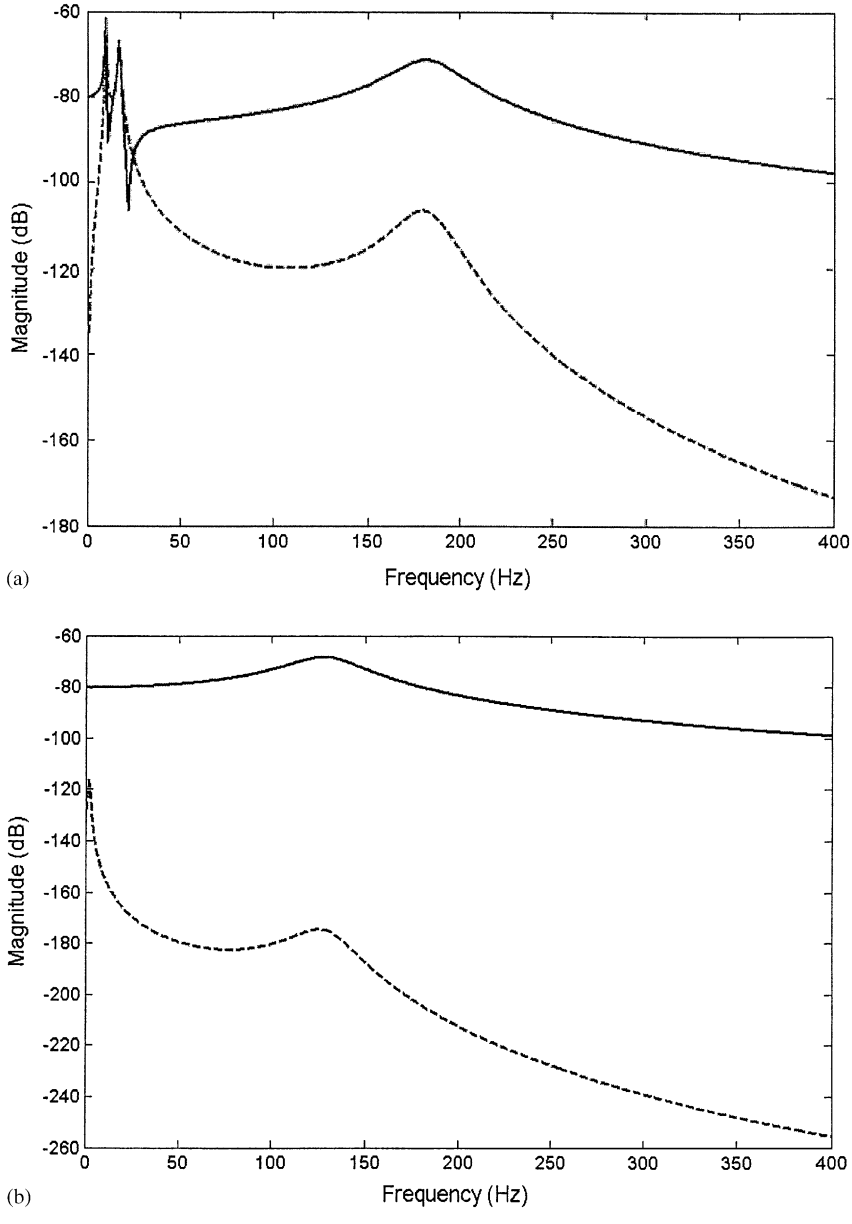

Figure 11. Frequency responses of the system in Figure 10: (a) $k_d = k_u$; (b) $k_d = 100k_u$ (——, frequency response of x_1/fc_1; – – – –, frequency response of x_2/f_{c1}).

Figure 11(a) shows the frequency responses of x_1/f_{c1} and x_2/f_{c1}, where k_d is equal to k_u. One can see that the level of the "crosstalk" x_2/f_{c1} is comparable with that of the "drive-point" responsex_1/f_{c1}. However, if k_d is much lager than k_u, the level of x_1/f_{c1} is also much greater than x_2/f_{c1}, as shown in Figure 11(b). This simulation indicates that the coupling among actuators can be reduced by using an upper mount much softer than the lower mount.

On the other hand, the effect of payload dynamics is also examined. For the 1-degree-of-freedom system of Figure 12(a), the transfer function between the control force

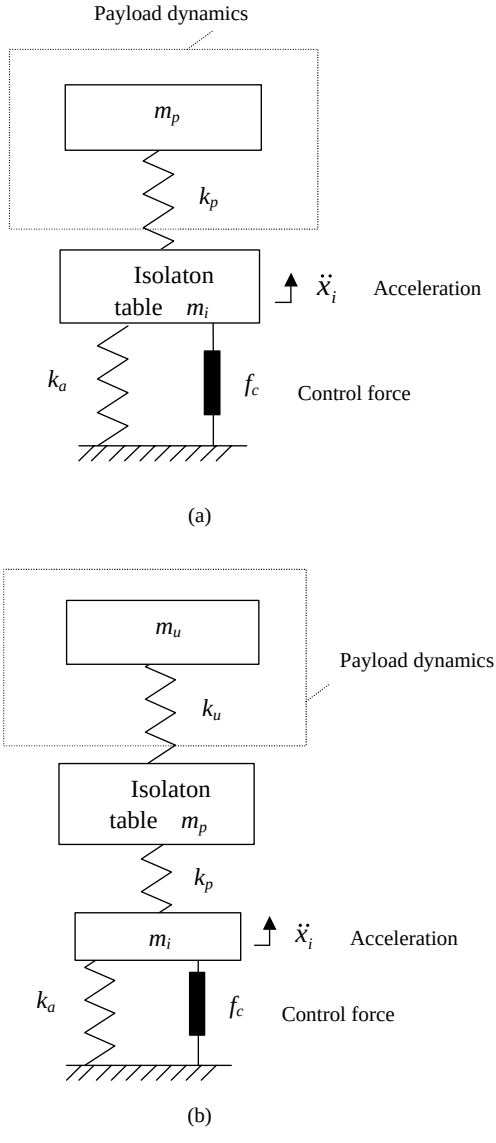

Figure 12. System with payload dynamics: (a) isolation table with payload dynamics; (b) isolation table with intermediate mass and payload dynamics.

f_c and the sensor $\ddot{x}_i$ can be written as

$$\frac{\ddot{x}_i}{f_c} = \frac{s^2/m_i(s^2 + k_p/m_p)}{s^4 + (k_p/m_p + (k_a + k_p)/m_i)s^2 + k_a k_p/m_p m_i} \tag{19}$$

It can be seen that pole–zero pairs are added into the transfer function due to the payload dynamics. If $k_a \gg k_p$, the relation of resonance frequencies between the additional poles and zeros can be approximated as

$$\omega_p^2 \approx \omega_0^2 \left(\frac{k_a}{k_a + k_p} \right). \tag{20}$$

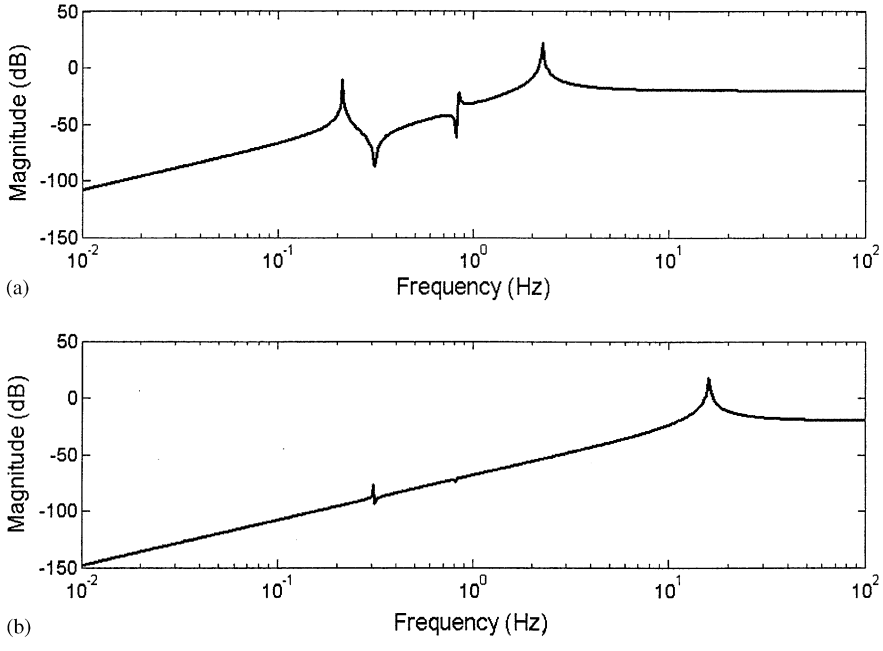

Figure 13. Frequency responses of $\ddot{x}_i/f_c$. (a) $k_a = k_p$; (b) $k_a = 100k_p$.

As the intermediate mass is added into the system, it becomes the structure as shown in Figure 12(b). The transfer function between the control force f_c and the sensor output $\ddot{x}_i$ turns out to be

$$\frac{\ddot{x}_i}{f_c} = \frac{N(s)}{D(s)} \tag{21}$$

where

$$N(s) = m_u m_p s^6 + [m_u(k_u + k_p) + k_u m_p]s^4 + k_u k_p s^2,$$

$$D(s) = m_u m_p m_i s^6 + m_u m_p m_i \left(\frac{k_a + k_p}{m_i} + \frac{k_i + k_p}{m_p} + \frac{k_u}{m_u}\right)s^4 + [(m_u + m_p)k_u(k_p + k_a) + (m_u + k_u)k_a k_p]s^2 + k_u k_a k_p.$$

If $k_a \gg k_p$, the peak due to payload dynamics can be cancelled, as shown in Figure 13. Thus, it can be concluded from this simulation, the influence of payload dynamics could be reduced by introducing intermediate masses to the system.

4.3. EXPERIMENTAL RESULTS OF CONFIGURATION 2

Two methods are employed for controller synthesis of configuration 2. One is the LQG controller with internal model and the other is the μ controller.

4.3.1. *LQG with internal model*

The parameters of LQG controller are $\mathbf{Q}_c = 2000 \times \mathbf{I}_{14\times14}$, $\mathbf{R}_c = \mathbf{I}_{3\times3}$, $\mathbf{Q}_f = 600 \times \mathbf{I}_{3\times3}$, and $\mathbf{R}_f = \mathbf{I}_{3\times3}$. Note that the dimension of $\mathbf{Q}_c$ is smaller than that of configuration 1. The

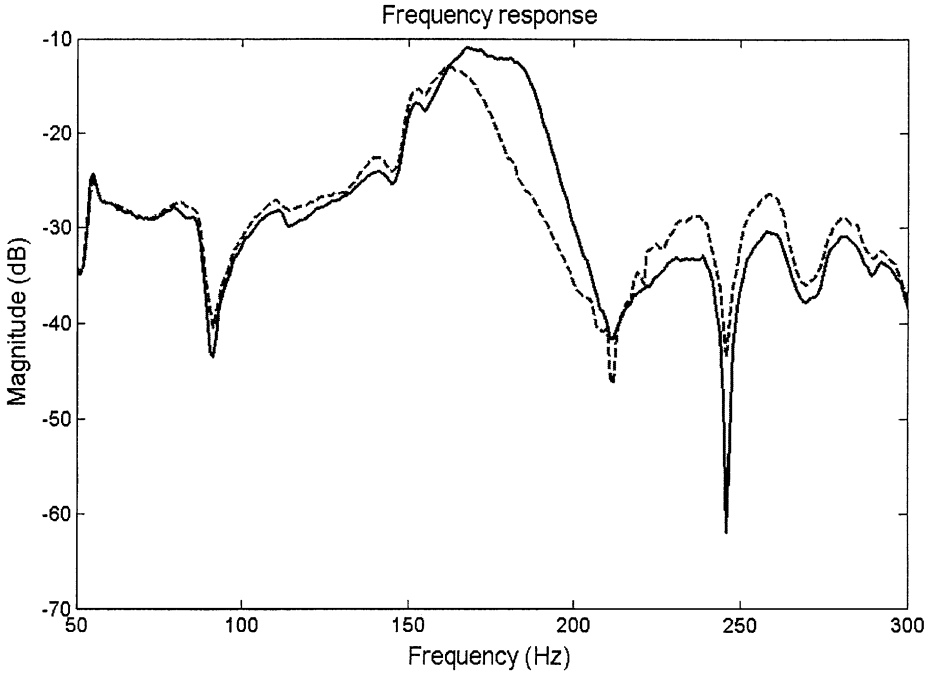

Figure 14. The experimental result of configuration 2 obtained using LQG control with internal model (——, control off, – – – –, control on).

transfer function of the internal model is

$$H(z) = \frac{0{\cdot}2556z^2 - 0{\cdot}2556}{z^2 - 0{\cdot}7528z + 0{\cdot}6429} \tag{22}$$

which corresponds to the resonance frequency of 180 Hz and the damping ratio of 20%. The experimental result is shown in Figure 14. Attenuation can be observed in the frequency range 165–213 Hz.Maximum attenuation is found to be 12·6 dB. In frequency range 218–300 Hz, the disturbance is amplified because of waterbed effect. However, the maximum amplification is only 3·9 dB that is smaller than configuration 1. It is noted that the LQG design is a somewhat *ad hoc* method and there is no guarantee whether the stability and performance margins are met. In addition, the design is based on the nominal plant that does not account for the high-frequency dynamics. From our experience, system may become unstable using LQG design, due to un-modelled high-frequency dynamics. To avoid instability, loop gain of the system should be restricted outside the control bandwidth, particularly when there is perturbations or uncertainties in the system. Incidentally, the following μ-synthesis is such a systematic and robust method able to fulfill this goal.

4.3.2. *μ-Synthesis*

Prior to μ-synthesis, the "size" of uncertainties must be characterized as a robustness specification. This is done by subtracting the modelled frequency response functions (by ERA) from the measured frequency response functions. The result is shown in Figure 15, where the so-calculated uncertainties (solid lines) are bounded by the associated uncertainty

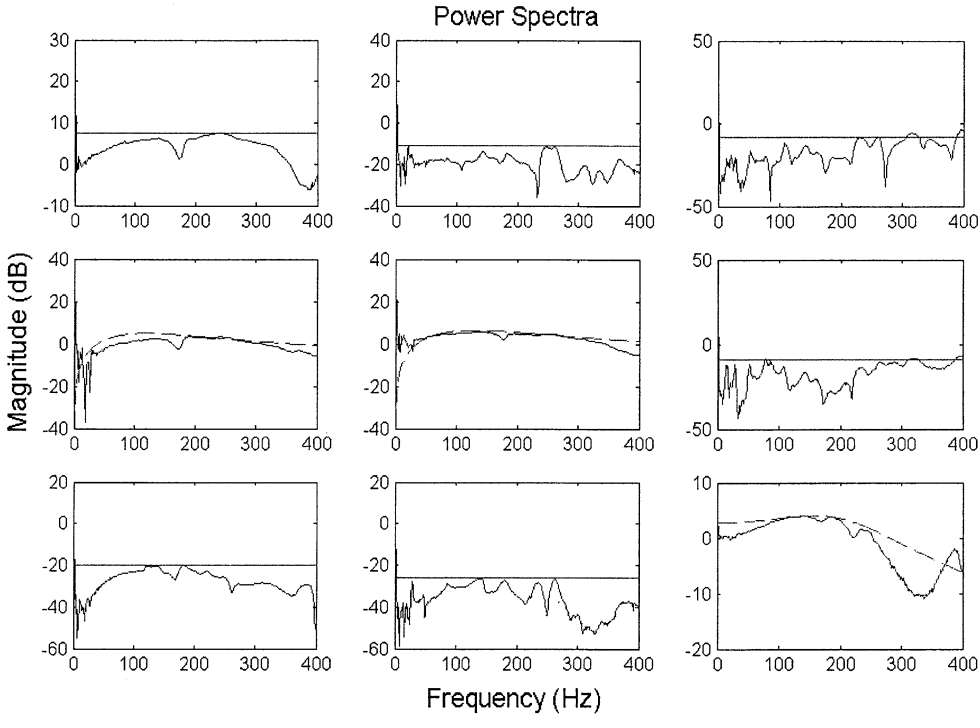

Figure 15. Spectra of uncertainties and the associated weights (——, uncertainty; – – – –, uncertainty weight).

weights (dash lines). The uncertainty weights are expressed in the following 3×3 matrix:

$$\mathbf{W}_{mult} = \begin{bmatrix} \dfrac{1{\cdot}516\text{e}006}{s^2 + 804s + 1{\cdot}011\text{e}006} & 0{\cdot}11 & 0{\cdot}11 \\ \dfrac{1900s}{s^2 + 1068s + 1{\cdot}141\text{e}006} & \dfrac{1{\cdot}617\text{e}006}{s^2 + 804s + 1{\cdot}011\text{e}006} & 0{\cdot}29 \\ 0{\cdot}26 & 0{\cdot}29 & \dfrac{1{\cdot}997\text{e}006}{s^2 + 1068s + 1{\cdot}141\text{e}006} \end{bmatrix}, \quad (23)$$

where the parameter α can be varied in order to gauge the effect of the weight on the closed-loop performance and robustness. In this experiment, $\alpha = 1, 0{\cdot}8, 0{\cdot}1$. Figure 16 shows the experimental results with respect to each α value. It is seen that the design with $\alpha = 1$ tends to be conservative and the performance is poor, as shown in Figure 16(a). In Figure 16(b), when α is reduced to 0·8, the performance is improved. However, Figure 16(c), when α is too small, the closed-loop system is nearly unstable. The robust performance index (the μ plot) with $\alpha = 0{\cdot}8$ and 0·1 are shown in Figure 17. It is desired to keep the μ values as small as possible such that the control design achieves robust performance. If α is too small, the maximum μ value becomes much greater than unity.

5. CONCLUSIONS

In this work, a DSP-based active isolation system has been developed. Numerical and experimental investigations are carried out to examine two control algorithms and two

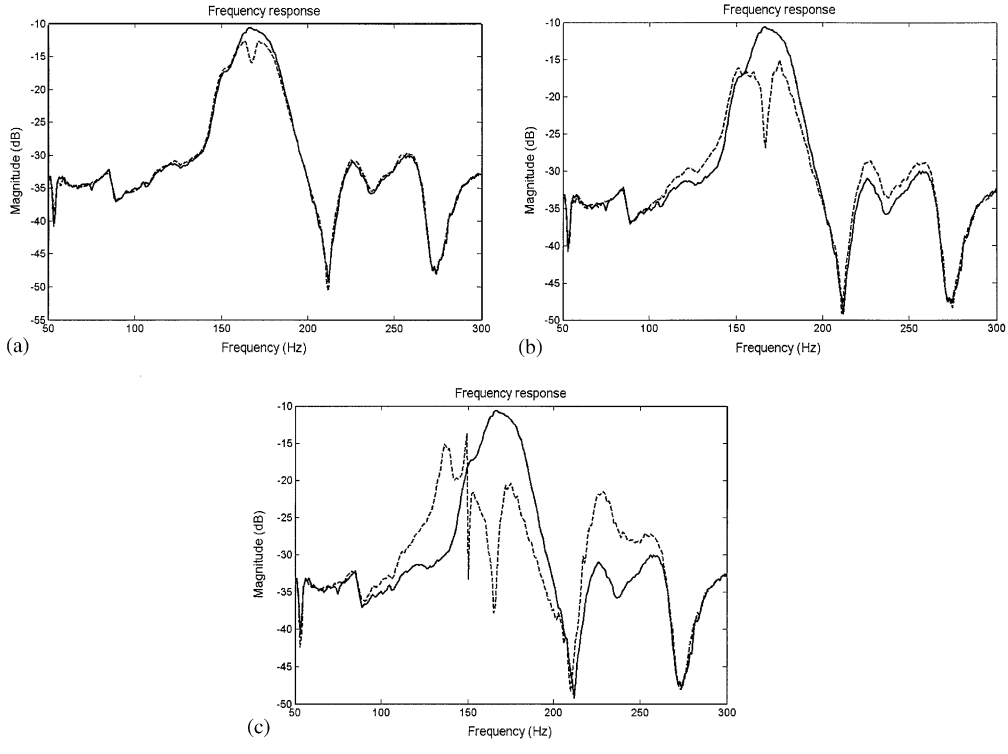

Figure 16. Experimental result with various gains of uncertainty weights: (a) $\alpha = 1$ (b) $\alpha = 0{\cdot}8$; (c) $\alpha = 0{\cdot}1$ (——, control off, – – – –, control on).

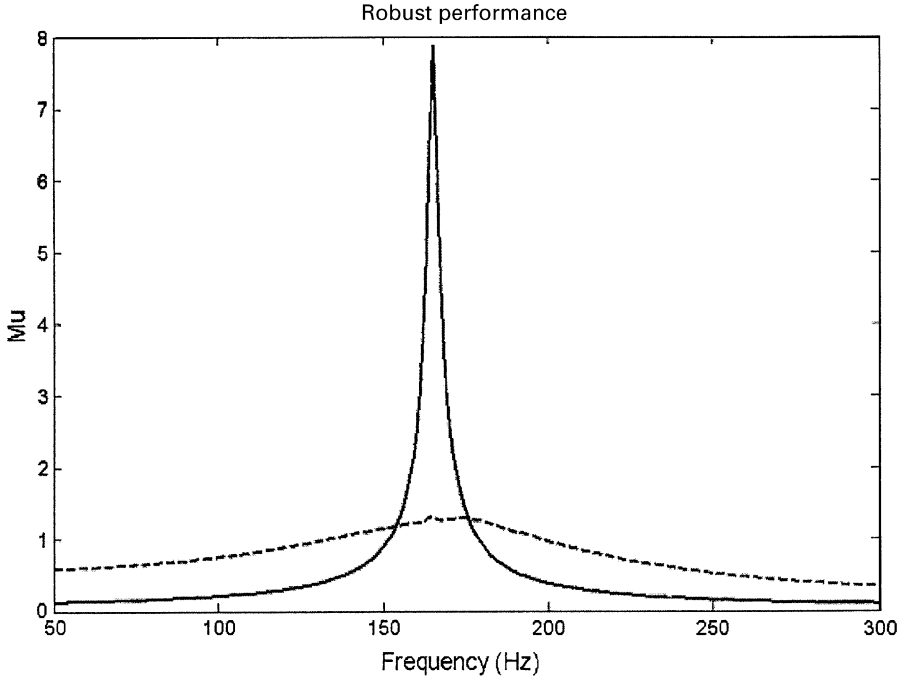

Figure 17. The μ plot of the controller (—— $\alpha = 0{\cdot}1$, – – – –, $\alpha = 0{\cdot}8$).

configurations. The results indicate that proper configuration is very crucial for entire control design. In particular, intermediate masses are shown to be useful in reducing the influence of payload dynamics and coupling among the actuators. LQG control and μ synthesis are employed in the controller synthesis. In LQG design, system may become unstable due to un-modelled high-frequency dynamics, whereas μ-synthesis is able to provide better robustness against uncertainties in the system.

There are some possible extensions of this research. Decoupling of the actuators could be enhanced mechanically or electronically to an extent such that the controller could be designed by a single-input and single-output basis. In the work, only narrowband performance has been achieved, but overall frequency-averaged attenuations are poor. It is suspected that the electromagnetic actuators are unable to deliver sufficient force output within a broad bandwidth. In the future, other types of actuators such as pneumatic or hydraulic actuator should be used for application with heavier payloads. In this work, only vertical motions are of concern. Other types of motions, e.g., in-plane motion should also be accommodated in the future research.

ACKNOWLEDGMENTS

The work was supported by the National Science Council in Taiwan, Republic of China, under the project number NSC 89-2212-E-009-007. The authors would like to thank Prof. Stephen Elliot of ISVR, University of Southampton, U.K., for his helpful suggestions and provision of reference [5].

REFERENCE

1. D. C. KARNOPP, M. J. CROSBY and R. A. HARWOOD 1974 *American Society of Mechanical Engineers, Journal of Engineering for Industry* **96**, 619–626. Vibration control using the semiactive force generators.
2. A. M. BEARD, D. W. SCHUBER and A. H. VON FLOTOW 1994 *Proceedings of the American Society of Mechanical Engineers, Winter Annual Meeting*, Chicago, IL. A practical product implementation of an active/passive vibration isolation system.
3. L. A. SIEVERS and A. H. VON FLOTOW 1988 *Proceedings of the 27th Conference on Decision and Control*, Austin, TX, 1032–1037. Linear control design for active vibration isolation of narrow band disturbances.
4. K. WATANABE, S. HARA, Y. KANEMITSU, T. HAGA, K. YANO, T. MIZUNO and R. KATAMURA 1996 *Proceedings of the 35th Conference on Decision and Control*, Kobe, Japan, pp. 1223–1228. Combination of H^{∞} and PI control for an electromagnetically levitated vibration isolation system.
5. S. M. KIM, S. J. ELLIOT and M. J. BRENNAN 2001 *IEEE Transactions of Control Systems and Techniques* **9**, 93–100. Decentralized control for multiple active vibration isolation.
6. H. L. LANGHAAR 1962 *Energy Methods in Applied Mechanics*. New York: John Wiley & Sons.
7. F. L. LEWIS and V. L. SYRMOS 1995 *Optimal Control*. New York: John Wiley & Sons.
8. K. GLOVER and J. DOYLE 1988 *System and Control Letters* **11**, 167-172. State-space formulate for all stabilizing controllers that satisfy an H_{∞} norm bound and relations to risk sensitivity.
9. J. C. DOYLE, K. GLOVER, P. P. KHARGONEHAR and B. A. FRANCIS 1989 *IEEE Transactions on Automatic Control* **34**, 831–847. State-space solution to standard H_2 and H_{∞} control problems.
10. G. J. BALAS, J. C. DOYLE, K. GLOVER, A. K. PACKARD and R. SMITH 1990 *μ-Analysis and Synthesis Toolbox: User's Guide*. Natick, MA: MUSYN and The Mathworks
11. C. T. CHEN 1984 *Linear System Theory and Design*. New York: Oxford University Press.
12. J. N. JUANG 1994 *Applied System Identification*. Englewood Cliffs, NJ: Prentice-Hall.
13. F. B. YEH and C. D. YANG 1992 *Post Modern Control Theory and Design*. Taiwan: Eurasia